Journal of Molecular Liquids 344 (2021) 117741

Contents lists available at ScienceDirect

Journal of Molecular Liquids

journal homepage: www.elsevier.com/locate/molliq

Enhancing skin permeation of nanoemulsions through associative polymeric micelles-mediated drop-to-skin dipolar interactions

Minchul Sung [a], Dae Hyun Shin [b], Hyo Jung Lee [b], Kyoung Hee Jang [b], Kyounghee Shin [a,c,*], Jin Woong Kim [a,*]

[a] School of Chemical Engineering, Sungkyunkwan University, Suwon 16419, Republic of Korea
[b] Research and Development Center, Cosmocos Corporation, Incheon 21698, Republic of Korea
[c] Convergence Research Center for Energy and Environmental Sciences, Sungkyunkwan University, Suwon 16419, Republic of Korea

ARTICLE INFO

Article history:
Received 7 August 2021
Revised 27 September 2021
Accepted 30 September 2021
Available online 2 October 2021

Keywords:
Nanoemulsion
Polymeric micelle
Skin permeation
Chain conformation
Dipolar interaction

ABSTRACT

This study presents a facile but useful methodology to improve the skin permeation of nanoemulsions through associative polymeric micelle (APM)-mediated drop-to-skin dipolar interactions. Amphiphilic triblock copolymers, poly(ethylene oxide)-b-poly(ε-caprolactone)-b-poly(ethylene oxide) (PEO-PCL-PEO), were co-assembled with lecithin to fabricate APMs. As model drug carriers, nanoemulsions were prepared using the same amphiphile composition. Dense-suspension rheological studies revealed that when APMs co-existed with nanoemulsions, the drop-to-drop association was predominantly influenced by the PEO chain conformation surrounding the APMs; shorter PEO chains reduced the APM-mediated nanoemulsion association due to weak chain conformation. The shorter PEO chains of the APMs promoted the drop-to-skin association. Therefore, APMs with short PEO chains aided the penetration of the nanoemulsion into the skin. These results highlight that manipulation of the nanoemulsion drop association is important and plays a role in enhancing dermal drug delivery performance.

Contents

* Corresponding authors at: School of Chemical Engineering, Sungkyunkwan University, Suwon 16419, Republic of Korea (K. Shin and J.W. Kim).
E-mail addresses: sca680@skku.edu (K. Shin), jinwoongkim@skku.edu (J.W. Kim).

https://doi.org/10.1016/j.molliq.2021.117741
0167-7322/

1. Introduction

Stratum corneum (SC), structured with combined lipid bilayers in the keratinized region, acts as a primary protection barrier against external hazardous factors [1]. This intrinsic function of SC makes transdermal drug delivery challenging [2,3]. Nano-drug delivery platforms, including lipid vesicles [4–6], polymeric micelles [7], nanoemulsions [8,9], and nanoparticles [10,11], have been developed to enhance transdermal delivery without damaging the skin structure by taking advantage of the high diffusivity of nanoscale drug carriers [12]. However, these typical diffusion-based delivery systems are still subject to SC skin barrier function, necessitating the development of technology to actively deliver drugs through the SC layer. The active transdermal drug delivery technology relies on inducing a strong mutual attraction between the drug carrier and the skin surface [13]. Therefore, nanocarriers decorated with skin-attractive biomolecules, including cell-penetrating peptides [14,15], antigens [16,17], DNA molecules [18], and SC lipids [19], can readily get adsorbed into the skin to help the delivery of the encapsulated drug.

Active transdermal delivery is more effective when a well-designed polymer is incorporated to induce physical adsorption [20–26]. For example, positively charged chitosan coated on solid nanoparticles improves transdermal drug permeation through electrostatic interaction with the negatively charged skin surface [27,28]. In addition, PEGylation of nanocarriers promotes their wetting on the skin surface due to the association of polyethylene glycol with SC lipids, thus improving skin penetration of the encapsulated drug [24,29]. These studies propose that hydrophilic associative polymers act as molecular linkers with the skin for delivery carriers. Polymeric micelles show high linking efficiency as colloidal linker complex fluids compared to single polymers because they can interact in all directions. The conformation of associative polymer chains at the periphery of micelles increases the possibility of interacting with the skin surface as well as with other micelles, which is the advantage of using a nanomicellar system with a corona structure over a single molecule system. Such a new transdermal delivery system not only allows significant improvement of drug delivery performance but also fine-tuning of the rheological behavior of complex biofluids.

Herein, we report a simple and practical approach to improve skin permeation of an active compound in an oil-in-water (O/W) nanoemulsion by employing associative polymeric micelles (APMs) as a mediator connecting emulsion drops with the skin surface. For this purpose, we prepared associative nanoemulsions (ANEs) that were formulated with the same amphiphiles, amphiphilic triblock copolymers (PEO-PCL-PEO) and lecithin, used for the fabrication of APMs. A common feature of these colloidal systems is the induction of dipole–dipole interactions between the terminal methoxy group of PEO blocks and the phosphorylcholine group of the hydrophilic head of lecithin. We investigated how the chain conformation of PEO blocks at the periphery of APMs affected the rheological behavior and water evaporation behavior of the ANEs. Consequentially, we demonstrated that the use of APMs with controlled chain conformations of PEO brushes plays an essential role in drop-to-skin dipolar interactions that eventually determine the skin penetration of an active compound.

2. Materials and methods

2.1. Materials

PEO-PCL-PEO triblock copolymers with different molecular weights were synthesized via a condensation reaction between methoxy-terminated poly(ethylene oxide) (mPEO) and poly(ε-caprolactone) (PCL). We used two types of PEO-PCL-PEO with block ratios of 2 k:2k:2k and 5 k:10 k:5k. mPEO (Mn = 2,000 g/mol and Mn = 5,000 g/mol), PCL (Mn = 2,000 g/mol and Mn = 10,000 g/mol), isophorone diisocyanate (IDPI), and dibutyltin dilaurate (DBTDL) were purchased from Sigma-Aldrich (USA). Lecithin was commercially available as Lipoid P75-3 (soybean lecithin, Lipoid Kosmetik AG, Germany) containing 70% hydrogenated phosphatidylcholine and 30% other components. Porcine skin with a thickness of 400 μm was purchased from Micropig Franz Cell Membrane (Korea). 3D human skin model Neoderm®-ED was purchased from Tego Science (Korea) and analyzed according to the manufacturer's instructions. PC-104 was obtained from the Amore Pacific (Korea). All other chemicals used were of reagent grade. Deionized (DI) double-distilled water was used in all experiments.

2.2. Preparation of ANEs and APMs

For the preparation of an ANE, 2.4 wt% of PEO_{5k}-PCL_{10k}-PEO_{5k} and 0.6 wt% of lecithin (Lipoid P75-3) were melted with 1,3-butylene glycol at 85 °C. Pre-heated 57% (w/v) DI water was then added to the melted mixture, and 40% (w/v) olive oil was slowly poured into the triblock copolymer-based aqueous mixture while homogenizing (ULTRA-TURRAX® T-25 basic dispersers, IKA, Japan) at 13,000 rpm for 2 min. This precursor emulsion was downsized by homogenization with a high-pressure homogenizer (MN400BF, Micronox, Korea) at a pressure of 1,000 bar for five cycles [30]. To obtain an APM, 2.4 wt% PEO-PCL-PEO and 0.6 wt% lecithin were first dissolved in tetrahydrofuran (THF) by sonication at 40 °C for 5 min. Then, 97 wt% of DI water was added dropwise while vigorously stirring the mixture at 100 μL/min using a syringe pump (Pump 11Elite, Harvard Apparatus, USA). Then, THF was completely removed from the APM dispersion by evaporation at 40 °C. APM-added ANE dispersions were produced by simple mixing of an APM dispersion to an ANE dispersion in a ratio of 1:9 (v/v). The size and zeta potential of both ANEs and APMs were measured by dynamic light scattering (DLS) with a He–Ne laser (632.8 nm) (ELS-Z, Otsuka Electronics, Japan). To avoid multiple scattering, all samples were diluted with DI water before each measurement. After negative staining of the samples with 1 wt% uranyl acetate, drop and micelle morphologies were observed using a transmission electron microscope (TEM; LIBRA 120, Carl Zeiss, Germany) operating at 120 kV.

2.3. Dense-suspension rheology studies

The rheological properties of APM-treated ANE fluids were observed in a concentrated suspension state using a DHR-3 rheometer (TA Instruments, USA). A cone-plate type geometry with a diameter of 40 mm and an angular gap of 2° was used with a gap of 54 μm. The evaporation of water from the test fluid during the measurement was prevented by surrounding the rheometer plate with a solvent trap. After equilibrating each test sample loaded on the plate for 30 min, the flow sweep and frequency sweep modes were operated. The flow sweep test was conducted by varying the shear rate from 0.1 to 100 1/s. The frequency sweep test was carried out at angular frequencies (ω) ranging from 0.1 to 100 rad/s with constant amplitude (γ = 1.0%). In all suspension rheology studies, the volume fraction of ANE + APM was set to 0.5 ± 0.01 by controlling evaporation of the aqueous continuous phase. The corrected oil volume fraction was determined using a moisture analyzer (MX-50, A&D, Japan).

2.4. Gravimetric determination of water evaporation rate

The evaporation rate was determined using Croll's model employing the gravimetric analysis method. A sample (50 μL)

was treated evenly on porcine skin with an area of 2 × 2 cm^2. The treated skin was placed in a desiccator with a constant internal environment (temperature = 25 °C; relative humidity = 40%). The changes in mass were recorded at 5 min intervals for 48 h using an electronic scale (Sartorius Lab Instruments GmBH & Co. KG, Germany, d = 0.1 mg) equipped with Weigh Anchor by Sartorius Hong Kong (version: 2.0). The free-water evaporation (FWE) stage was fitted using the linear regression method. The transition time t_c was determined when the linear regression coefficient was 0.98. The mass change during bound water evaporation (BWE) was fitted to exponential decay, $m\ (t) = m_0 + Ae^{-bt}$, to analyze the BWE stage. The evaporation rate at the BWE stage was obtained by differentiating the mass change with respect to t and dividing it into the mass at t_c to compensate for the difference in water concentration between each sample.

2.5. Noninvasive visualization of skin penetration

For the skin penetration study, we topically treated porcine skin with APM-treated ANE fluids with a fluorescent drug probe (Nile red) in oil drops. After 24 h of treatment, we collected a series of fluorescence images stacked along the z-axis from the skin surface using a confocal laser scanning microscope (CLSM, TCS SP8 HyVolution, Leica Microsystems, USA). The wavelength of the light source was 532 nm for excitation of the Nile red fluorescence probe with a UV–Vis laser port UV/405. The scanned pattern was focused using an objective lens (40×, ZEISS, Germany). The fluorescent signal of the collected images was analyzed for obtaining the intensity profile using the ImageJ program.

2.6. In vitro skin penetration study

In vitro skin penetration of APM-treated ANE fluids was carried out following the TG No.428, OECD guidelines. In this study, APM-treated ANEs that contained 0.01 wt% of ceramide PC-104 were prepared in oil drops as a probe drug. For the non-vehicle control, 0.01 wt% of PC-104 was dissolved in methanol. The 3D human skin model with SC, epidermis, and dermis (thickness = 1.00–1.20 mm) was prepared after washing with phosphate-buffered saline for 30 min. Then, the skin model was placed between the donor and receptor chambers, with SC facing the donor chamber. The area of the diffusion cell was 2.54 cm^2. After topological treatment of 20 μL of the sample at different time intervals (3, 6, 9, and 24 h), the penetration of PC-104 through the skin model was quantified using high-performance liquid chromatography (HPLC) fitted with a 100–5 C18 column (Kromasil, 4.6 × 250 mm, 5 μm, Sweden), coupled to UV–Vis and MS detection at 205 nm wavelength (Agilent 1260 VWD, USA), equipped with a binary pump (Agilent 1260 Quat Pump VL, USA) and an automatic injector (Agilent 1260 ALS, USA). The flow rate was 1 mL/min. Methanol and water were used as mobile phases. The significant retention time of PC-104 was 2.7 min. The area under curve was integrated by Chromeleon software (Dionex). All values are the mean ± standard deviation of three determinations. The statistical significance (p-value) of the data was analyzed by a one-way ANOVA test using Origin 8.5 software (OriginLab Co., Northampton, USA) and $p < 0.01$ was considered statistically significant.

3. Results and discussion

3.1. Fabrication and characterization of ANEs and APMs

It is known that APMs can associate with each other through direct interactions between hydrophilic polymer brushes on their surface that depend on the chemistry, chain length, and chain conformation of hydrophilic polymer chains, in addition to the dispersion medium conditions, including pH, temperature, and osmolality. In this study, we apply the favorable properties of APMs to propose a methodology that can further enhance the skin penetration performance of ANEs, thus imparting new functional applications to conventional emulsion formulations. For this, we synthesized two types of triblock copolymers with different PEO chain lengths: PEO_{2k}-PCL_{2k}-PEO_{2k} and PEO_{5k}-PCL_{10k}-PEO_{5k} (Fig. 1a). The hydrophobic blocks were selected according to the PEO chain length to match the hydrophilic-lipophilic balance between the two triblock copolymers. Each PEO-PCL-PEO was co-assembled with Lipoid P75-3 to form APM_{6k} and APM_{20k}, respectively (Fig. 1b–d). The ANE was prepared using PEO_{5k}-PCL_{10k}-

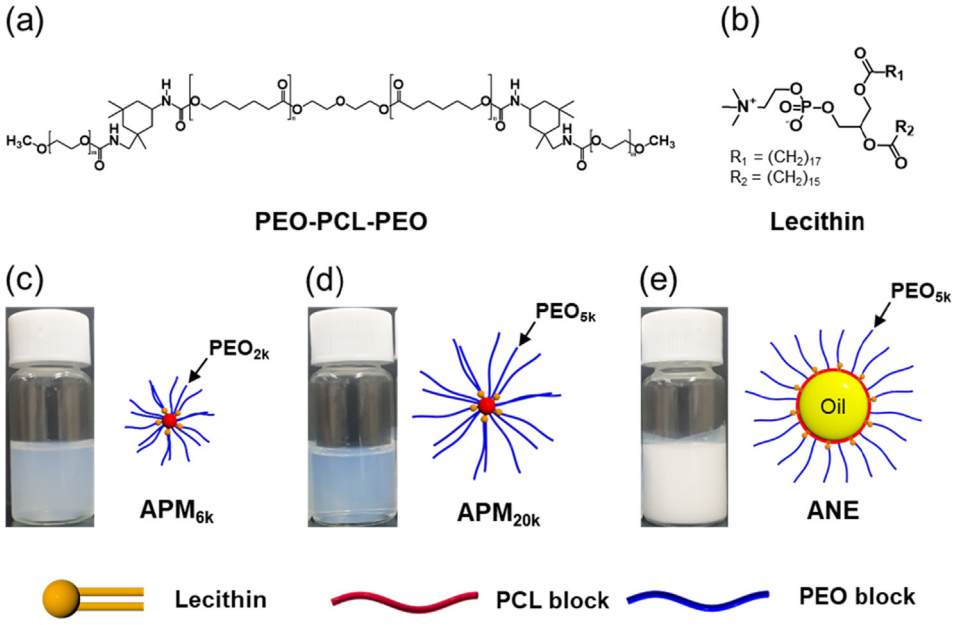

Fig. 1. Chemical structures of (a) PEO-*b*-PCL-*b*-PEO and (b) lecithin (Lipoid P75-3). The appearance of APMs and ANEs prepared with PEO-b-PCL-b-PEO and Lipoid P75-3: (c) PEO_{2k}-PCL_{2k}-PEO_{2k} and Lipoid P75-3, (d) PEO_{5k}-PCL_{10k}-PEO_{5k} and Lipoid P75-3, and (e) PEO_{5k}-PCL_{10k}-PEO_{5k} and Lipoid P75-3.

PEO_{5k} and Lipoid P75-3 (Fig. 1e). The co-assembled Lipoid P75-3 on both APMs and ANEs was capable of inducing the dipole–dipole interactions between the methoxy group at the tail end of the PEO blocks and the phosphorylcholine group on the head [31]. Particularly, Lipoid P75-3 was chosen because it not only has skin compatibility, but also induces the dipole–dipole attraction.

The ANE and APMs prepared in this study were characterized by DLS, zeta potential, and TEM analyses. The ANE was prepared by co-assembling PEO_{5k}-PCL_{10k}-PEO_{5k} and Lipoid P75-3, which formed the smallest and most stable emulsion system at a hydrodynamic size of 400 nm. This information was used throughout the study. To minimize any effect of particle size variation, we prepared APMs with similar particle sizes by fixing the composition of PEO-PCL-PEO/Lipoid P75-3 to 8/2 (w/w) and applying high-pressure homogenization at a pressure of 1,000 bar for five cycles, that enabled tuning their hydrodynamic size to approximately 100 nm (Fig. 2a). The zeta potential was detected at −35 mV for the ANE and −15 mV for the APMs. Such negative zeta potentials of the ANE and APMs are due to the incorporation of Lipoid P75-3 (Fig. 2b) [32,33]. Although APM_{20k} showed slightly higher zeta potential values than APM_{6k} because of the shielding of the APM surface by longer PEO brushes [34], the difference was negligible at the 5 mV level. In the TEM observation, the ANE nanodrops showed a slightly distorted morphology, which implies that the PEO-PCL-PEO/Lipoid P75-3 formed a resilient composite polymer film at the O/W interface (Fig. 2c). The APMs presented a blurred round-shaped particle morphology but had similar particle sizes, regardless of the molecular structure of PEO-PCL-PEO (Fig. 2d–e). The above analysis shows that the APMs prepared as intended in this study have a particle size that is sufficiently smaller than that of ANE, and that there is no significant difference in particle size and surface potential between the two; only the PEO chain length is different.

3.2. Understanding of APM-mediated drop-to-drop interactions of ANE fluids

To evaluate how the addition of APMs affects the inter-drop association in the ANE system, we investigated the dense-suspension rheological behaviors of ANE fluids in the presence of APMs [35]. All the ANE fluids were concentrated to 50% volume. No phase separation of ANE drops was observed even at such a high oil volume fraction because the resilient polymer film formed at the O/W interface structurally stabilizes the nanoemulsion drops [30]. As the ANE drops show higher mutual attraction at high concentrations, their dipolar interactions can be characterized more clearly. We observed that the incorporation of APM_{6k} into the ANE fluids at 25 °C lowered both $\acute{G}$ and G'' by approximately one unit, whereas the incorporation of APM_{20k} increased them (Fig. 3a–b). This implies that APM_{6k} interaction with emulsion

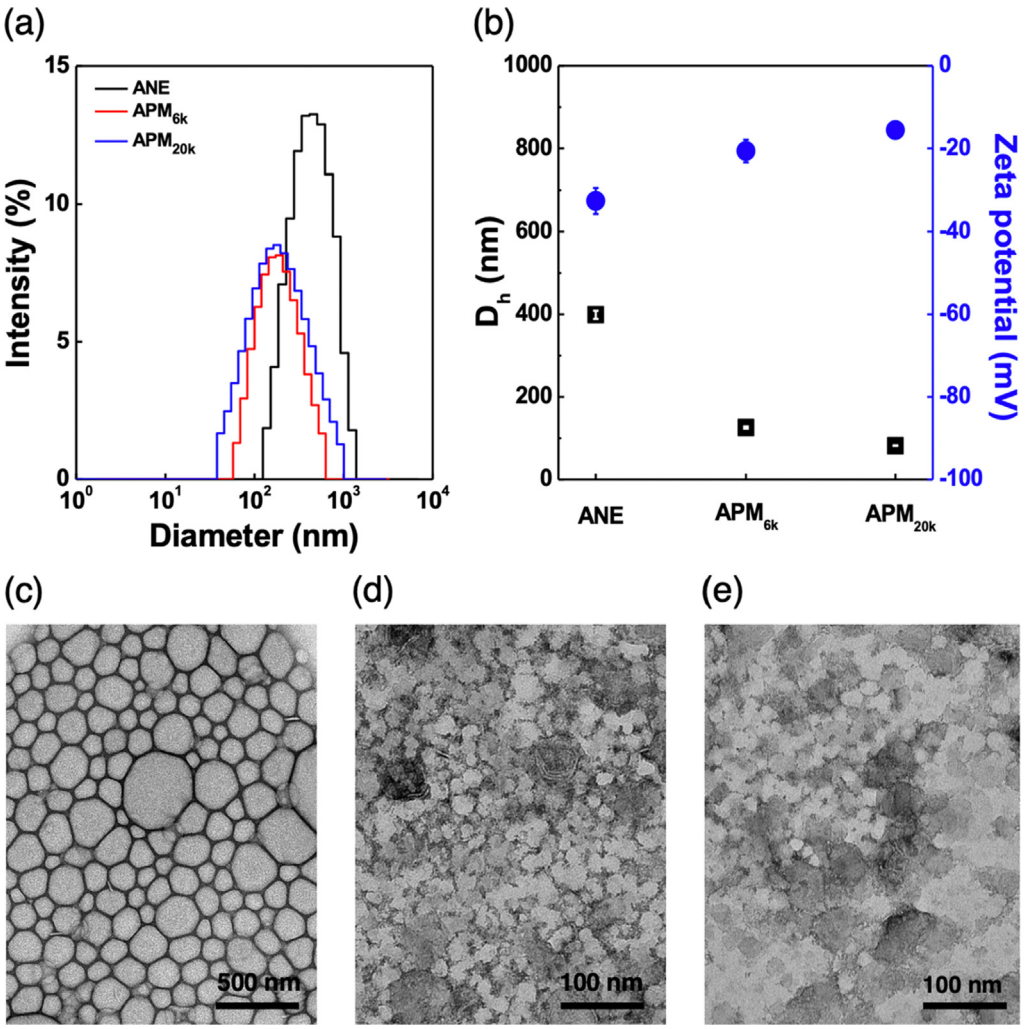

Fig. 2. (a) Size distribution of ANE and APMs. (b) Hydrodynamic size and zeta potential of ANE and APMs. TEM images of (c) ANE, (d) APM_{6k}, and (e) APM_{20k}.

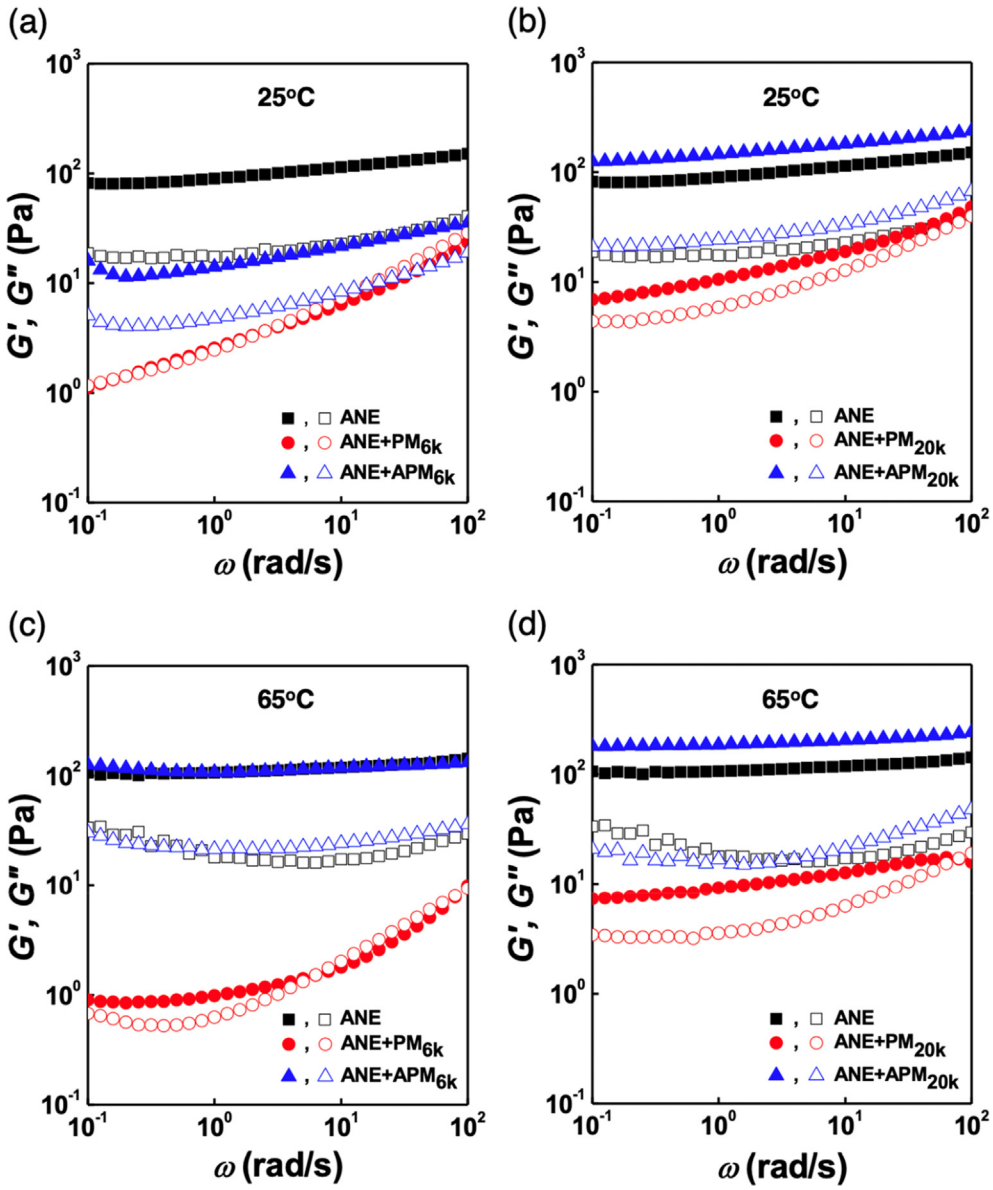

Fig. 3. Storage modulus ($\acute{G}$) and loss modulus (G'') against frequency changes for ANE fluids containing (a) APM_{6k} at 25 °C, (b) APM_{20k} at 25 °C, (c) APM_{6k} at 65 °C, and (d) APM_{20k} at 25 °C.

drops was weaker than that of APM_{20k} due to the limited conformation of PEO chains, thus making the fluid less elastic. As expected, PMs made of only block copolymers did not show any ability to make the fluid more attractive, which is comparable to the effect of adding APMs. To confirm whether the difference in rheological behavior according to the change in PEO chain length is due to chain conformation, we investigated the dense-suspension rheological behavior of ANE fluids at an elevated temperature. As the PEO chains dissolved in water collapse at the lower critical solution temperature (LCST, 60 °C), they changed their conformation from an elongated state to a coiled state near the LCST [36]. The APM_{6k}-treated ANE showed higher moduli at 65 °C than at 25 °C. As the short PEO chains coil, the van der Waals attraction between the droplets seems to be enhanced. Interestingly, we observed that the APM_{20k}-treated ANE fluid maintained its original rheological properties against the PEO chain collapse, which can be attributed to the effective entanglement of long PEO chains. These results suggest that the PEO chain conformation on the APMs plays an important role in controlling the APM-mediated inter-drop association of the ANE drops.

3.3. Water evaporation behavior of APM-treated ANE fluids

The APM-mediated drop-to-drop interaction presumably influences the water retention capacity of the ANE fluids on the skin surface. To figure out this, we examined the water evaporation rate on the skin topically treated with APM-treated ANE fluids. An aliquot of the ANE fluid was spread evenly on the porcine skin, and the mass change caused by water evaporation was monitored as a function of time. Applying the Croll's model [37,38] to the mass change, as shown in Fig. 4, the water evaporation pattern of ANE fluids is composed of FWE during the early stage and BWE during the later stage. The FWE of the APM_{20k}-treated ANE fluid, determined from the slope of the early stage of evaporation, was the lowest, establishing an even longer timescale. This suggests that thinning of the APM_{20k}-treated ANE fluid film by drying was

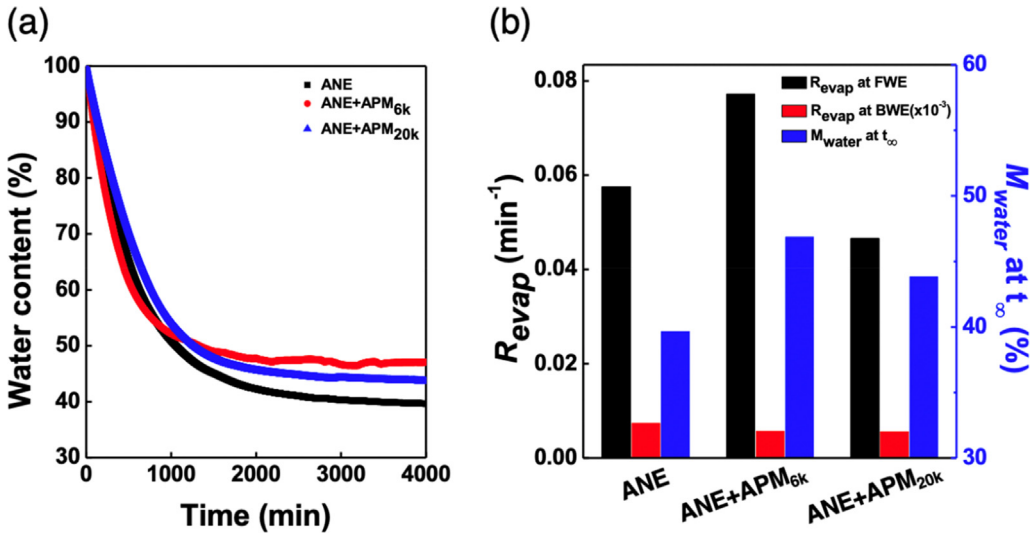

Fig. 4. **(a)** Water evaporation profiles of test samples on porcine skin as a function of time. Temperature and relative humidity were precisely controlled at 25 °C and 40%, respectively. (b) Water holding parameters obtained during the second evaporation stage. The evaporation rate at BWE was obtained by differentiating the mass change with respect to t and then dividing this value by the mass of water at the starting point of the BWE stage.

limited due to the favorable drop-to-drop association, thus hindering the dipolar interaction between the ANE droplets and skin lipids. This interpretation is reliable because the water content of the APM_{20k}-treated ANE fluid was lowest at the BWE stage. In our study, the water content of the APM_{6k}-treated ANE fluid was highest at both t_c and t_∞. This means that APM_{6k} having short PEO chains induces the drop-to-skin association rather than drop-to-drop association, facilitating the adhesion of emulsion drops onto the skin (see Table 1).

3.4. Visualization of skin penetration behaviors

To visualize the skin penetration profile of APM-added ANEs through the skin, we topically treated porcine skin with ANEs containing Nile red [39–41] as a fluorescent drug probe and captured images along the z-axis of the skin using CLSM. After 24 h of topical treatment, the transdermal delivery behavior of the drug probe was analyzed for fluorescence intensity at the depth of the SC layer (20 μm). Images of the skin scanned by CLSM at different depths showed that the drug probe distribution of the APM_{6k}-treated ANE was detected in deeper skin layers, which is comparable to other ANEs (Fig. 5). For a quantitative comparison, the fluorescence intensities were plotted against the z-direction of the skin depth, as shown in Fig. 6. The fluorescence intensity of APM_{6k}-treated ANE peaked at a depth of 10 μm whereas the other ANEs peaked at 5 μm. The accumulated fluorescence intensity of APM_{6k}-treated ANE increased by approximately 27%. In contrast, the APM_{20k}-treated ANE showed no significant change in the fluorescence intensity over the entire skin depth, while showing low intensity. Moreover, its accumulated fluorescence intensity was approximately half that of APM_{6k}-treated ANE. In the dense-suspension rheology study, we confirmed that APM_{20k} effectively enhanced the association between ANE drops and APM_{6k}. From the perspective of transdermal absorption of drug-containing nanodroplets, the stronger drop-to-drop attraction of the ANE lowers the chances of drop-to-skin attraction. Therefore, it was interpreted that the incorporation of APM_{5k} led to relatively weak drop-to-drop attraction and enhanced skin penetration of drug-containing nanodroplets.

3.5. Improved skin penetration performance of APM-treated ANEs

To further confirm the skin penetration behaviors of APM-treated ANEs, in vitro skin penetration studies were performed with 3D human skin in Franz diffusion cells. Ceramide was incorporated in the oil phase of all the ANE samples as a probe drug. HPLC analysis was conducted to quantify ceramide in the receptor solution collected at different time points (Fig. 7). It was noted that the peak integrations of ceramide observed over 9 h were not significant across the samples, and their intensities were also very low. However, noticeable differences were observed 24 h after application, showing that the peak integrations of ceramide were significant for the APM_{6k}-treated ANE, followed by ANE, and finally by APM_{20k}-treated ANE: this order followed the order of the skin penetration profiles. Intriguingly, the peak integration of APM_{20k}-treated ANE was slightly lower than that of the control. This implies that the skin penetration of the ANE drops hindered the strong association with APM_{20k}. It is evident that the introduction

Table 1
Parameters calculated from water evaporation profiles.

Sample	R_{evap} at FWE (min^{-1})	T_c (min) [b]	M_{water} at t_c (%) [c]	R_{evap} at BWE ($\times10^{-3}$, min^{-1}) [d]	M_{water} at t_∞ (%)
ANE	0.0575	769	55.74	0.0887	39.67
ANE/APM_{6k}	0.0772	495	61.78	0.0688	46.87
ANE/APM_{20k}	0.0466	967	54.98	0.0669	43.83

[a]FWE is the free-water evaporation stage. [b]Time taken to change from FWE to BWE stage. [c]M_{water} is the mass of remaining water. [d]R_{evap} is the evaporation rate obtained by fitting the mass change data using nonlinear regression during the BWE stage.

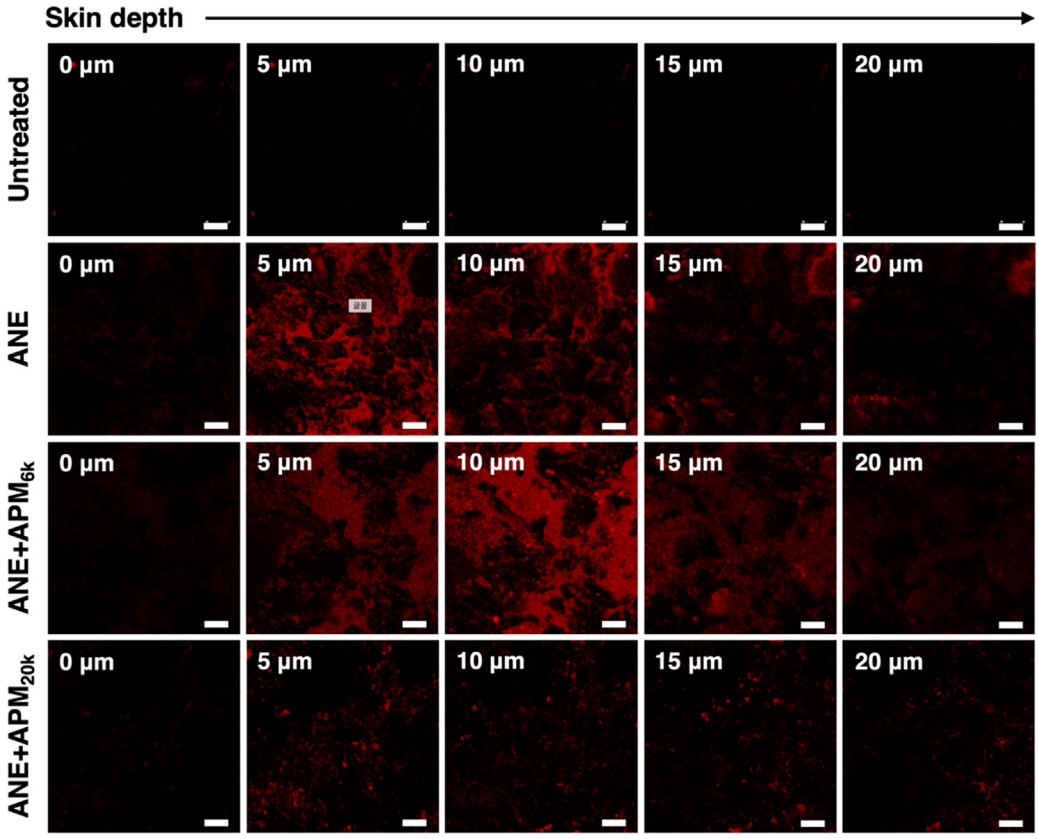

Fig. 5. (a) CLSM images of porcine skin along the z-direction after topical treatment with ANEs. The fluorescence dye was Nile red. The scale bar is 50 μm.

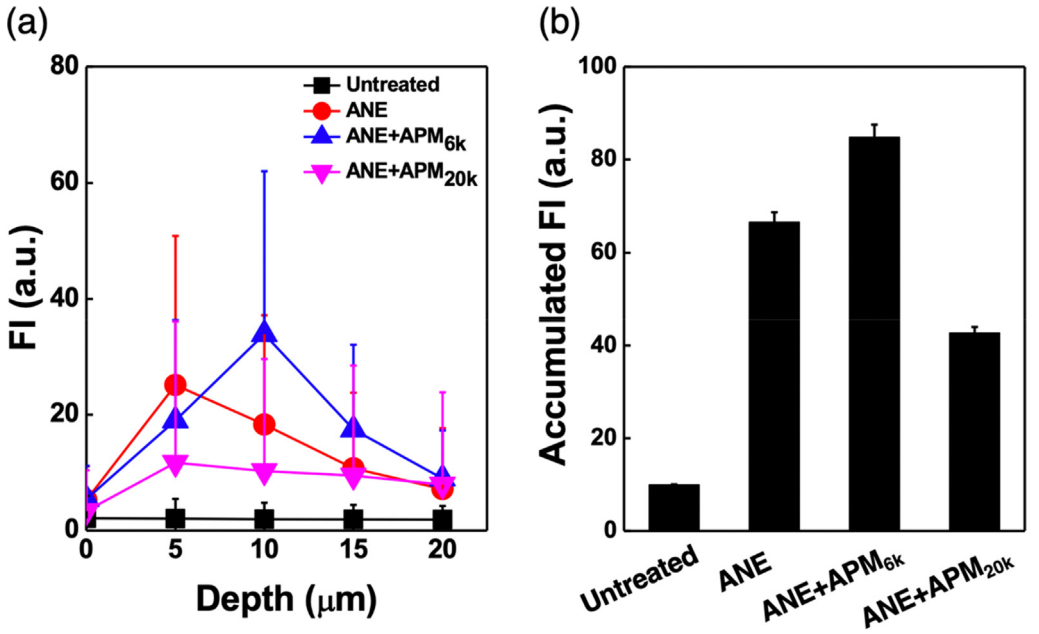

Fig. 6. (a) Fluorescence intensity (FI) and (b) accumulated fluorescence intensity versus skin penetration depth profiles after topically treating the porcine skin with Nile-red-loaded ANEs through the SC layer (0–20 μm).

of APM_{6k} to the ANE enhanced the skin penetration of ANE drops, whereas the introduction of APM_{20k} retarded the skin penetration. The APM_{6k}-aided improved skin penetration of the ANE is closely related to the intercellular penetration of weakly percolated nanodrops, which leads to more rapid diffusion due to less elastic properties.

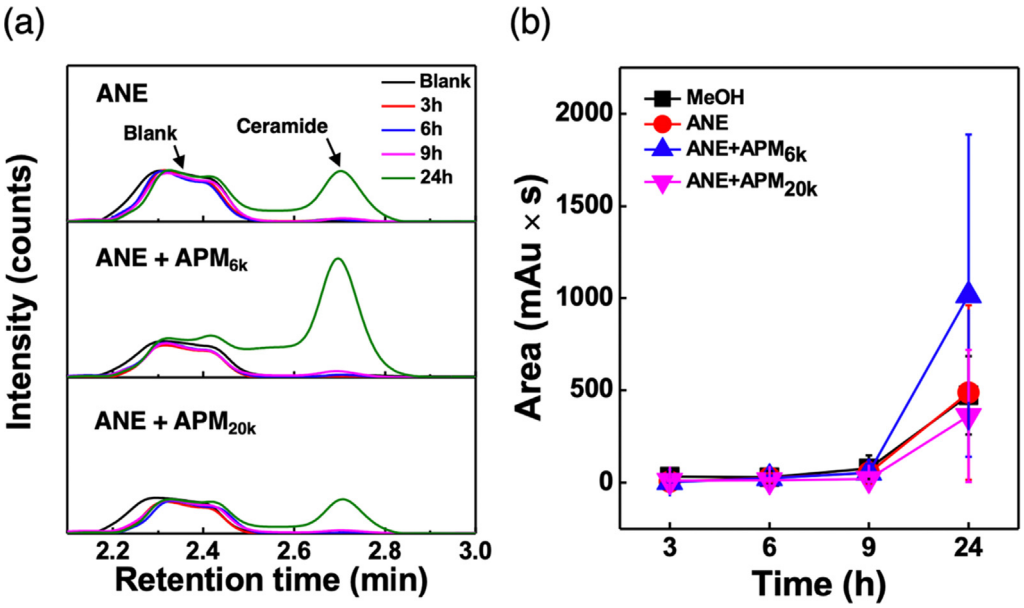

Fig. 7. (a) High-performance liquid chromatogram and (b) peak integration of skin-penetrated ceramide-loaded ANE fluids. The characteristic retention time of ceramide was 2.7 min. Ceramide dissolved in methanol was used as the control. Values are the mean ± standard deviation of three determinations. (**p < 0.01).

4. Conclusions

In summary, we introduced a facile and effective strategy for improving skin penetration of ANE by inducing a favorable drop-to-skin association. The key to our approach is to introduce APMs into the ANE fluids because APMs induce a strong mutual attraction between ANE drops and the skin surface. Our dense-suspension rheological and water evaporation analyses revealed that the PEO chain conformation on the APMs determines the favorable drop-to-skin association of ANE fluids. Finally, we showed that APMs with short PEO chains enhanced the skin penetration of the nanoemulsion. We expect that these findings will pave the way for the development of an advanced transdermal delivery system for pharmaceutical and personal care products.

CRediT authorship contribution statement

Minchul Sung: Formal analysis, Visualization, Writing – original draft. **Dae Hyun Shin:** Formal analysis. **Hyo Jung Lee:** Investigation. **Kyoung Hee Jang:** Methodology. **Kyounghee Shin:** Methodology, Writing – original draft, Writing – review & editing. **Jin Woong Kim:** Conceptualization, Writing – original draft, Writing – review & editing, Supervision.

Declaration of Competing Interest

The authors declare that they have no known competing financial interests or personal relationships that could have appeared to influence the work reported in this paper.

Acknowledgments

This research was supported by the National Research Foundation of Korea (NRF) grant funded by the Korea government (MSIT) (NRF-2019R1A2C1086383) and by Korea Initiative for fostering University of Research and Innovation Program of the National Research Foundation (NRF) funded by the Korean government (MSIT) (No.2020M3H1A1077095).

References

[1] A.M. Champagne, A. Munoz-Garcia, T. Shtayyeh, B.I. Tieleman, A. Hegemann, M.E. Clement, J.B. Williams, Lipid composition of the stratum corneum and cutaneous water loss in birds along an aridity gradient, J. Exp. Biol. 215 (2012) 4299–4307.
[2] M. Qindeel, M.H. Ullah, D. Fakhar Ud, N. Ahmed, A.U. Rehman, Recent trends, challenges and future outlook of transdermal drug delivery systems for rheumatoid arthritis therapy, J. Control Release 327 (2020) 595–615.
[3] M.C. Pena-Juarez, O.R. Guadarrama-Escobar, J.J. Escobar-Chavez, Transdermal Delivery Systems for Biomolecules, J. Pharm. Innov. (2021) 1–14.
[4] I.A. Chacko, V.M. Ghate, L. Dsouza, S.A. Lewis, Lipid vesicles: A versatile drug delivery platform for dermal and transdermal applications, Colloid Surf. B-Biointerfaces 195 (2020) 14.
[5] D.E. Large, R.G. Abdelmessih, E.A. Fink, D.T. Auguste, Liposome composition in drug delivery design, synthesis, characterization, and clinical application, Adv. Drug Deliv. Rev. 176 (2021) 113851.
[6] A.S. Almurshedi, M. Radwan, S. Omar, A.A. Alaiya, M.M. Badran, H. Elsaghire, I. Y. Saleem, G.A. Hutcheon, A novel pH-sensitive liposome to trigger delivery of afatinib to cancer cells: Impact on lung cancer therapy, J. Mol. Liq. 259 (2018) 154–166.
[7] J. Yan, Z. Ye, M. Chen, Z. Liu, Y. Xiao, Y. Zhang, Y. Zhou, W. Tan, M. Lang, Fine tuning micellar core-forming block of poly(ethylene glycol)-block-poly (epsilon-caprolactone) amphiphilic copolymers based on chemical modification for the solubilization and delivery of doxorubicin, Biomacromolecules 12 (2011) 2562–2572.
[8] V.K. Rai, N. Mishra, K.S. Yadav, N.P. Yadav, Nanoemulsion as pharmaceutical carrier for dermal and transdermal drug delivery: Formulation development, stability issues, basic considerations and applications, J. Control Release 270 (2018) 203–225.
[9] D.M. Mostafa, A.A. Kassem, M.H. Asfour, S.Y. Al Okbi, D.A. Mohamed, T.-S. Hamed, Transdermal cumin essential oil nanoemulsions with potent antioxidant and hepatoprotective activities: In-vitro and in-vivo evaluation, J. Mol. Liq. 212 (2015) 6–15.
[10] E. Blanco, H. Shen, M. Ferrari, Principles of nanoparticle design for overcoming biological barriers to drug delivery, Nat. Biotechnol. 33 (2015) 941–951.
[11] T.S. Anirudhan, B.S. Bini, V. Manjusha, Glycyrrhetinic acid conjugated zein capped aminated mesoporous silica nanoparticle-based dual drug delivery system for liver: A pH-dependent triggered release, J. Mol. Liq. 340 (2021) 116852.
[12] C. Pegoraro, S. MacNeil, G. Battaglia, Transdermal drug delivery: from micro to nano, Nanoscale 4 (6) (2012) 1881–1894.
[13] N.X. Wang, H.A. von Recum, Affinity-based drug delivery, Macromol. Biosci. 11 (3) (2011) 321–332.
[14] D. Park, J.Y. Lee, H.K. Cho, W.J. Hong, J. Kim, H. Seo, I. Choi, Y. Lee, J. Kim, S.-J. Min, S.-H. Yoon, J.S. Hwang, K.J. Cho, J.W. Kim, Cell-Penetrating Peptide-Patchy Deformable Polymeric Nanovehicles with Enhanced Cellular Uptake and Transdermal Delivery, Biomacromolecules 19 (7) (2018) 2682–2690.
[15] J.H. Cho, J.Y. Kang, S. Kim, H.R. Baek, J. Kim, K.-S. Jang, J.W. Kim, Skin protein-derived peptide-conjugated vesicular nanocargos for selected skin cell targeting and consequent activation, J. Mater. Chem. B 9 (24) (2021) 4956–4962.

[16] D. Mishra, P.K. Mishra, V. Dubey, S. Dabadghao, N.K. Jain, Evaluation of uptake and generation of immune response by murine dendritic cells pulsed with hepatitis B surface antigen-loaded elastic liposomes, Vaccine 25 (2007) 6939–6944.
[17] J. Lu, X. Liu, Y.P. Liao, X. Wang, A. Ahmed, W. Jiang, Y. Ji, H. Meng, A.E. Nel, Breast Cancer Chemo-immunotherapy through Liposomal Delivery of an Immunogenic Cell Death Stimulus Plus Interference in the IDO-1 Pathway, ACS Nano 12 (2018) 11041–11061.
[18] A. Matsumoto, Y. Takahashi, R. Ariizumi, M. Nishikawa, Y. Takakura, Development of DNA-anchored assembly of small extracellular vesicle for efficient antigen delivery to antigen presenting cells, Biomaterials 225 (2019) 119518.
[19] J.B. Lee, M. Sung, M. Noh, J.E. Kim, J. Jang, S.J. Kim, J.W. Kim, Effective association of ceramide-coassembled lipid nanovehicles with stratum corneum for improved skin barrier function and enhanced skin penetration, Int. J. Pharm. 579 (2020) 119162.
[20] R.E.R. Ramirez, E.S. Orth, C. Pires, S.F. Zawadzki, R.A. de Freitas, DODAB-DOPE liposome surface coating using in-situ acrylic acid polymerization, J. Mol. Liq. 330 (2021) 115689.
[21] H. Takeuchi, H. Kojima, H. Yamamoto, Y. Kawashima, Polymer coating of liposomes with a modified polyvinyl alcohol and their systemic circulation and RES uptake in rats, J. Control Release 68 (2) (2000) 195–205.
[22] J. Shin, P. Shum, J. Grey, S.-I. Fujiwara, G.S. Malhotra, A. González-Bonet, S.-H. Hyun, E. Moase, T.M. Allen, D.H. Thompson, Acid-labile mPEG-vinyl ether-1,2-dioleylglycerol lipids with tunable pH sensitivity: synthesis and structural effects on hydrolysis rates, DOPE liposome release performance, and pharmacokinetics, Mol. Pharm. 9 (11) (2012) 3266–3276.
[23] O. D'Agostini-Junior, C.L. Petkowicz, A.G. Couto, S.F. de Andrade, R.A. Freitas, Simultaneous in situ monitoring of acrylic acid polymerization reaction on N-carboxymethyl chitosan using multidetectors: Formation of a new bioadhesive and gastroprotective hybrid particle, Mater. Sci. Eng. C Mater. Biol. Appl. 31 (3) (2011) 677–682.
[24] H. Otsuka, Y. Nagasaki, K. Kataoka, Self-assembly of poly(ethylene glycol)-based block copolymers for biomedical applications, Curr. Opin. Colloid In. 6 (1) (2001) 3–10.
[25] S.-H. Kim, J. Nam, J.W. Kim, D.-H. Kim, S.-H. Han, D.A. Weitz, Formation of polymersomes with double bilayers templated by quadruple emulsions, Lab Chip 13 (7) (2013) 1351–1356.
[26] J.W. Kim, J.Y. Ko, J.B. Jun, I.S. Chang, H.H. Kang, K.D. Suh, Multihollow polymer microcapsules by water-in-oil-in-water emulsion polymerization: morphological study and entrapment characteristics, Colloid Polym. Sci. 281 (2003) 157–163.
[27] M. Rahbar, A. Morsali, M.R. Bozorgmehr, S.A. Beyramabadi, Quantum chemical studies of chitosan nanoparticles as effective drug delivery systems for 5-fluorouracil anticancer drug, J. Mol. Liq. 302 (2020) 112495.
[28] D.M. Ridolfi, P.D. Marcato, G.Z. Justo, L. Cordi, D. Machado, N. Duran, Chitosan-solid lipid nanoparticles as carriers for topical delivery of tretinoin, Colloids Surf. B Biointerfaces 93 (2012) 36–40.
[29] A. Lalloz, M.A. Bolzinger, S. Briancon, J. Faivre, J.M. Rabanel, A. Garcia Ac, P. Hildgen, X. Banquy, Subtle and unexpected role of PEG in tuning the penetration mechanisms of PLA-based nano-formulations into intact and impaired skin, Int. J. Pharm. 563 (2019) 79–90.
[30] J.Y. Lee, M. Sung, H. Seo, Y.J. Park, J.B. Lee, S.S. Shin, Y. Lee, K. Shin, J.W. Kim, Temperature-responsive interdrop association of condensed attractive nanoemulsions, J. Ind. Eng. Chem. 86 (2020) 158–166.
[31] K. Shin, G. Gong, J. Cuadrado, S. Jeon, M. Seo, H.S. Choi, J.S. Hwang, Y. Lee, A. Fernandez-Nieves, J.W. Kim, Structurally Stable Attractive Nanoscale Emulsions with Dipole-Dipole Interaction-Driven Interdrop Percolation, Chem. Eur. J. 23 (2017) 4292–4297.
[32] Y. Yegin, J.K. Oh, M. Akbulut, T. Taylor, Cetylpyridinium chloride produces increased zeta-potential on Salmonella Typhimurium cells, a mechanism of the pathogen's inactivation, NPJ. Sci. Food 3 (2019) 21.
[33] D.E. Park, D. Adhikari, R. Pangeni, V.K. Panthi, H.J. Kim, J.W. Park, Preparation and Characterization of Callus Extract from Pyrus pyrifolia and Investigation of Its Effects on Skin Regeneration, Cosmetics 5 (2018) 71.
[34] T. Gorner, R. Gref, D. Michenot, F. Sommer, M.N. Tran, E. Dellacherie, Lidocaine-loaded biodegradable nanospheres. I. Optimization of the drug incorporation into the polymer matrix, J. Control Release 57 (1999) 259–268.
[35] D.H. Kim, J.W. Kim, S.G. Oh, J. Kim, S.H. Han, D.J. Chung, K.D. Suh, Effects of nonionic surfactant on the rheological property of associative polymers in complex formulations, Polymer 48 (2007) 3817–3821.
[36] S. Hocine, M.-H. Li, Thermoresponsive self-assembled polymer colloids in water, Soft Matter 9 (25) (2013) 5839–5861.
[37] S. Croll, Drying of latex paint, J. coat. technol. 58 (1986) 41–49.
[38] S.T. Eckersley, A. Rudin, Drying Behavior of Acrylic Latexes, Prog. Org. Coat. 23 (4) (1994) 387–402.
[39] W.-R. Lee, S.-C. Shen, I.A. Aljuffali, Y.-C. Li, J.-Y. Fang, Erbium-yttrium-aluminum-garnet laser irradiation ameliorates skin permeation and follicular delivery of antialopecia drugs, J. Pharm. Sci. 103 (11) (2014) 3542–3552.
[40] S. Hong, J. Park, J.E. Kim, D. Park, S. Kim, J.Y. Kang, J.Y. Lee, W.J. Hong, H. Jeon, H. o. Lee, J.W. Kim, Fabrication of cell membrane-adhesive soft polymeric nanovehicles for noninvasive visualization of epidermal-dermal junction-targeted drug delivery, Int. J. Pharm. 565 (2019) 233–241.
[41] J.S. Baek, C.V. Pham, C.S. Myung, C.W. Cho, Tadalafil-loaded nanostructured lipid carriers using permeation enhancers, Int. J. Pharm. 495 (2015) 701–709.